Check for updates

# Boosting the ultraviolet shielding and thermal retardancy properties of unsaturated polyester resin by employing electrochemically exfoliated e-GO nanosheets

Son Anh Nguyen,[†ac] Thuc Quang Dong,[†ac] Mai Quan Doan,[†b] Ngoc Huyen Nguyen,[b] Tuan Anh Nguyen, [b] Xuan Dinh Ngo, [b] Anh-Tuan Pham[*cd] and Anh-Tuan Le [*bd]

In this work, a series of unsaturated polyester resin (UPRs)/electrochemically exfoliated graphene oxide (e-GO) polymer nanocomposites with different ratios of e-GO (0.05, 0.1, 0.15, and 0.2 wt%) were prepared *via* an *in situ* polymerization method. The surface morphology and structural and chemical properties of the original UPR and UPR/e-GO nanocomposites were characterized by scanning electron microscopy (SEM), X-ray diffraction (XRD), and fourier transform infrared spectroscopy (FTIR). The positive influence of e-GO nanosheets on the mechanical properties, thermal stability, and anti-UV aging performance of UPR/e-GO nanocomposites was demonstrated by thermogravimetric analysis (TGA), differential scanning calorimetry (DSC), and dynamic mechanical analysis (DMA). The obtained results showed that the incorporation of e-GO nanosheets within the UPR matrix, despite the addition of e-GO at as low as 0.2 wt% comprehensively improves the advanced functional properties of UPR/e-GO nanocomposites as compared to the original UPR. In addition, artificial weathering testing of quartz-based artificial stone using UPR/e-GO 0.2 wt% showed excellent UV-resistant efficiency, supporting the use of e-GO nanosheets as an additive in manufacturing the industrial-scale UPRs-based artificial quartz stone samples for real outdoor applications.

## 1. Introduction

Among the wide range of polymers, unsaturated polyester resin (UPR) is an important kind of thermosetting material, which has been extensively used worldwide due to its many intriguing properties.[1,2] UPR polymers can offer typical properties such as good mechanical properties, high thermal and heat stability, low shrinkage curing with a less volatile product, low price, processability, and availability of various grades.[3–5] From an industrial perspective, UPR has been utilized for a number of different applications such as pipes, tanks, sanitary ware, and high-performance polymers for the building, automotive, marine, and electric industries.[6,7] Natural and artificial weathering tests can give insights into the influence of important aging factors like solar ultraviolet (UV) radiation, thermal degradation, photo-

oxidation, and humidity (liquid and vapor) on the chemical, physical, and mechanical properties of UPR materials.[8–10] According to many previous studies,[7,11–13] UV radiation is one of the most critical weathering factors because UV light is capable of initiating photochemical processes that lead to discoloration and degradation. When exposed to UV radiation, the interaction of UPR materials with highly energetic radiation can cause the formation of free radicals.[7,14,15] These active intermediates are energetically higher than the strength of chemical bonds (O–O, C–C, C–N, H–O, *etc.*) in UPR polymer,[15] therefore triggering chain scission, crosslinking, side group abstraction, branching, and rearrangement in UPR molecular.[16–18] As a result, the main chains of UPR polymer may be broken down and degraded into fragments. UPR polymer undergoes UV-stimulated photo-oxidative reactions that result in the failure of commercial products-based UPR such as cracking, discoloring, fading, or disintegrating,[15,19] leading to the limitation in many outdoor applications of UPR-based commercial products. From the manufacturing point of view, it is imperative to find more effective methods to improve the UV resistance, mechanical, and thermal of UPR-based novel high-performance products.

Nowadays, many studies have been concentrated on combining polymer science and nanotechnology to solve

[a]Vicostone Joint Stock Company, Phenikaa Group, Hanoi 10000, Vietnam

[b]Phenikaa University Nano Institute (PHENA), Phenikaa University, Hanoi 12116, Vietnam. E-mail: tuan.leanh@phenikaa-uni.edu.vn

[c]Faculty of Biotechnology, Chemical and Environmental Engineering, Phenikaa University, Hanoi 12116, Vietnam

[d]Faculty of Materials Science and Engineering, Phenikaa University, Hanoi 12116, Vietnam. E-mail: fattuan@phenikaa-uni.edu.vn

† N. A. Son, D. Q. Thuc and M. Q. Doan contributed equally to this work.

inherent problems and induce new properties in conventional polymeric materials.[20] The union of nanomaterials and polymer matrices can be termed as polymer nanocomposites.[20,21] Polymer nanocomposites are materials having at least one phase remaining in the nanometer range (within 100 nm), which can be made by incorporating nanoscopic inorganic particles into different polymer matrices. The use of active nanomaterials as reinforcement or additives in polymer nanocomposites not only exhibits significantly improved most of the desired properties when compared to original polymers or conventional polymers composites but also potentially offers new properties depending upon the nanomaterials present in the resultant polymeric materials.[22–24] It is expected that polymer nanocomposites could enhance many important properties such as UV resistance, mechanical properties, thermal stability, electrical properties, fire resistance, chemical resistance, optical properties, *etc.* Among these properties, improving the UV resistance of UPR is of great interest to scientists and industrial manufacturers over the world. Hengzhi Chen *et al.*[25] synthesized UPR/ZnO nanocomposites and evaluated their mechanical and UV-shielding properties. Their findings reveal that the addition of a mere 3 wt% ZnO to the UPR matrix led to a remarkable increase in tensile and bending strengths by 91.4% and 71.3%, respectively, compared to pure UPR. Furthermore, with just 1 wt% of ZnO, the UPR/ZnO nanocomposite demonstrated a substantial improvement in UV absorbance within the 300–400 nm range, without a significant impact on UPR transparency. These results highlight the potential of UPR/ZnO nanocomposites as effective UV-shielding materials. Guirong Peng *et al.*[26] also used ZnO nanomaterials to study the influence of different ZnO contents on the strength and stability of UPR after exposure to UV irradiation. The results have shown that the proper content of ZnO added into UPR could lessen the UV degradation process of the matrix resin and can also increase the impact strength of the material. M. T. Rahman *et al.*[27] fabricated UPR matrix-based polymer nanocomposites by incorporating Fe$_2$O$_3$, TiO$_2$, and NiFe$_2$O$_4$ nanoparticles into the polymer matrix. The obtained results indicated the maximum improvement was found in tensile strength (21.62%), Young's modulus (6.56%), Vickers microhardness number, and the lowest optical energy band gap (18.96%) for NiFe$_2$O$_4$ dispersed nanocomposite, light absorbance in UV-vis range (30.38%) for Fe$_2$O$_3$ incorporated nanocomposite, and the highest direct current electrical conductivity and the lowest resistivity in Fe$_2$O$_3$ + TiO$_2$ + NiFe$_2$O$_4$ loaded nanocomposite. However, one of the main drawbacks of the inclusion of semiconductor nanomaterials into polymer matrices is its free radical production when it is exposed to UV irradiation.[28,29] Chain scission is a result of free radical diffusion among polymer chains.[17,18] In addition, most of the semiconductor nanomaterials used are in the form of particles, which is not conducive to improving the UV shielding ability of the matrix polymer.

Graphene oxide (GO) is a monolayer of graphite oxide formed from the oxidation of graphite by strong oxidizing agents. Due to its excellent properties such as absorbing most of the UV light to generate carriers (electron–hole pairs),[30] efficient heat absorption and dissipation,[31] and combined with low

photocatalytic activity (although GO has a good ability to absorb UV radiation),[32] GO-filled polymer nanocomposite is expected to enhance mechanical properties, thermal behavior, antiultraviolet aging properties. A well-known property of GO is its unique structure, characterized by graphene planes that incorporate diverse oxygen functional groups on the basal planes and carboxylate groups along the edges,[32,33] which may make them have the ability to strongly interact with micro-molecules or polymers, thus improving the dispersion of GO nanosheets in UPR matrix.[34,35] Hana G. Attiya *et al.*[36] successfully fabricated a UPR/graphene nanocomposite, employing graphene nanoparticles as a reinforcing agent *via* a mechanical mixing method. The resultant samples produced better mechanical and thermal properties as well as glass transition temperature than the original resin samples. To improve the flame retardant performance compared to original UPR, Wang *et al.*[37] synthesized a Cu$_2$O–TiO$_2$-GO reinforced composite that improved fire resistance and significantly reduced emissions of toxic substances such as CO, benzene, and aromatic compounds when burnt. Nidhin Divakaran and colleagues[38] fabricated surface-modified GO/UPR nanocomposites by incorporating the functionalized GO into the UPR matrix *via in situ* polymerization. The obtained materials displayed highly improved thermal, mechanical, and electrical properties, despite the addition of f-GO as low as 0.04 wt%. These studies show that GO enabled the comprehensive property enhancement of the UPR-based polymer nanocomposites. However, there have been no published studies documenting the improvement in the UV resistance of the UPR matrix when using GO nanosheets. Furthermore, the GO fabrication methods mentioned above cannot be produced in large quantities, making it difficult to apply on an industrial scale.

In this study, a simple, green, and cost-effective approach to produce industrial-scale GO nanosheets *via* electrochemical exfoliation of graphite and its applications in comprehensive property enhancement of the GO/UPR nanocomposites has been reported. UPR/e-GO polymer nanocomposites were prepared by using different electrochemically exfoliated GO (e-GO) loading amounts (0.05, 0.1, 0.15, and 0.2 wt%) assimilated within the UPR matrix through *in situ* polymerization method. The thermal and mechanical properties and UV resistance of UPR/e-GO nanocomposites materials have been studied in detail. UPR/e-GO nanocomposites with optimized e-GO loading amounts have been evaluated for real application in artificial quartz stone samples and their UV-resistant durability.

## 2. Experimental methods

### 2.1 Chemical

Maleic anhydride (MA, 99.8%) was produced by Nan-Ya Plastics Co., Ltd., (Taiwan). Phthalic anhydride (PA, 99.8%) was purchased from Continental Petrochemicals Co., Ltd., (Thailand). Propylene glycol (PG) and diethylene glycol (DEG, 99.9%) were provided by Petronas Chemicals Group Berhad (Malaysia). Hydroquinone (HQ, 99.0%) was supplied by Beijing DM Oilfield High-Tech Co., Ltd., China. Styrene solvent was from Wee Tee Tong Chemicals (Singapore). *Tert*-butyl peroxybenzoate (TBPB)

and cobalt(II) octoate (10%) were purchased from AkzoNobel, (Belgium). 3-(Trimethoxysilyl)propyl methacrylate silane was provided by Wacker chemie (Belgium). Ammonium sulfate ($(NH_4)_2SO_4 > 98\%$) was purchased from Shanghai Chemical Reagent. Double distilled water was used throughout the experiments.

## 2.2 Electrochemically synthesized e-GO nanomaterials

The e-GO nanosheets were exfoliated by using a electrochemical method, as reported in the previous study.[39] Two pure identical graphite plates were immersed in a 700 mL glass beaker filled with an electrolyte consisting of 0.1 M ammonium sulfate $(NH_4)_2SO_4$ aqueous solution. Subsequently, a direct current (DC) voltage source (7 V) was supplied to the anode and cathode electrodes under magnetic stirring for 8 hours.

## 2.3 UPR/e-GO composite materials preparation

In the present study, UPR was prepared from the polymerization reaction of MA, PA, PG, and DEG. In a 1000 mL, four-neck flask fitted with a mechanical stirrer, inlet to inert $N_2$ gas, thermometer, water condenser, and calibrated distillate collector, the precursors containing MA, PA, PG, and DEG with the mole ratios of 0.86 : 0.26 : 0.4 : 0.6 were added with mechanical stirring until a homogeneous solution was obtained. The UPR/e-GO polymer nanocomposites were prepared by the same method with a slight modification. The different loading of e-GO (0.05,

**Table 1** Experimental parameters of the UPR and UPR/e-GO fabrication process

| Samples | Mol ratio | | | | |
|---|---|---|---|---|---|
| | PG | DEG | MA | PA | e-GO wt% |
| UPR | 0.86 | 0.26 | 0.4 | 0.6 | 0.00 |
| UPR/e-GO 0.05% | 0.86 | 0.26 | 0.4 | 0.6 | 0.05 |
| UPR/e-GO 0.10% | 0.86 | 0.26 | 0.4 | 0.6 | 0.10 |
| UPR/e-GO 0.15% | 0.86 | 0.26 | 0.4 | 0.6 | 0.15 |
| UPR/e-GO 0.20% | 0.86 | 0.26 | 0.4 | 0.6 | 0.20 |

0.1, 0.15, and 0.2 wt%) were dispersed within the PG by mechanical stirring. The detailed preparation conditions for five UPR and UPR/e-GO samples are listed in Table 1. All the reaction mixtures were heated at 150–220 °C for about 12 hours under a nitrogen flow to prevent the color change of the obtained samples. The acid value of the mixture is continuously monitored throughout the reaction. The reaction was stopped when the acid value of the mixture was lower than 30 mg KOH per g. When the temperature of the reaction mixture cooled down to 90–100 °C, 0.2 wt% hydroquinone and 33–35 wt% styrene were added and thoroughly mixed. The viscosity of the as-prepared UPR is 600–650 cps (23 °C) (Scheme 1).
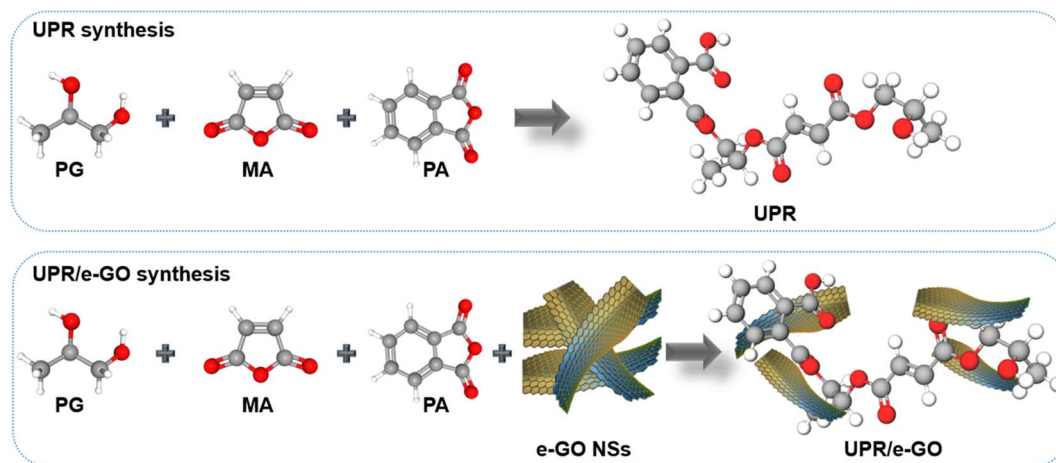
## 2.4. Preparation of specimens

In order to investigate the mechanical, thermal properties and UV resistance of UPR and UPR/e-GO materials, 1 wt% methyl ethyl ketone peroxide (MEKP) as an initiator and 0.01 wt% cobalt salts as an accelerator, was added to the mixture and further mixed well. The prepared resin mixtures were poured into a mold coated with Teflon with the dimensions 120 mm × 12 mm × 2 mm for curing. Curing occurs during heating the resin mixtures at 80 °C for 45 minutes, followed by drying at 120 °C for 60 minutes.

## 2.5 Artificial quartz stone samples preparation and UV resistant measurement

Scheme 2 illustrates the manufacturing process of grain-reinforced composites (quartz-based artificial stone). The current industrial production of artificial quartz stone is mainly through a process called "vacuum vibro-compression", which includes vacuum vibration and compression method. In this process, according to the designed ratio, coarse aggregate from quartz sandstones of different sizes such as ≤0.045 mm, 0.1 ÷ 0.3 mm, and 0.4 ÷ 0.6 mm are evenly dispersed in the mixer with agitator. Then, the curing agent, the curing accelerator, and UPR/e-GO polymer nanocomposites with the appropriate amount were added, mixed thoroughly. After that, coarse aggregate from quartz sandstone with a size ≤0.045 mm was
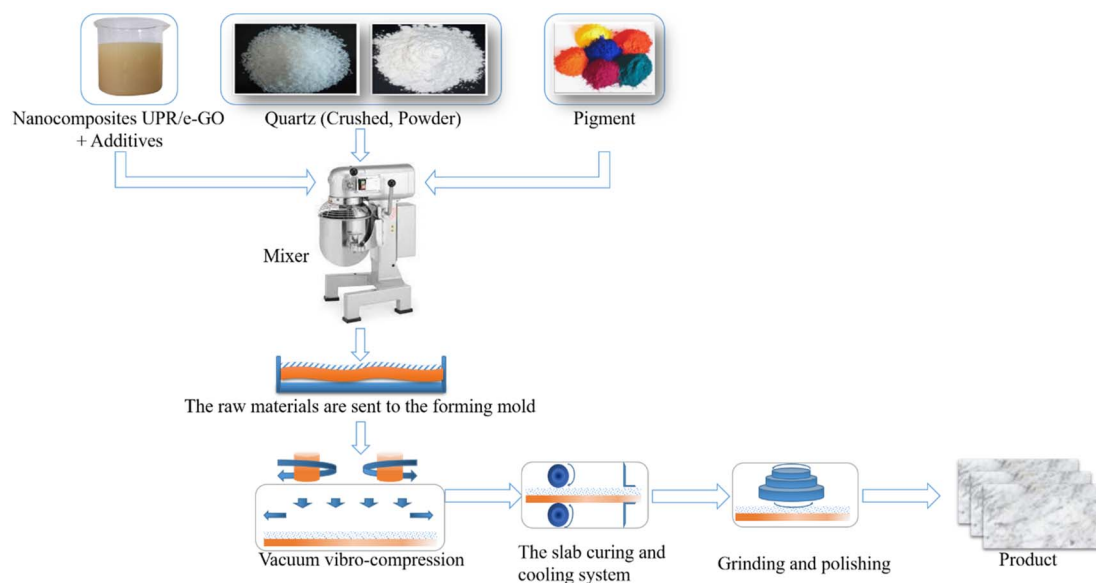


**Scheme 1** Schematic illustration of the synthesis process of UPR and UPR/e-GO nanocomposites.

**Scheme 2** Schematic illustration of the manufacturing process of grain-reinforced composites (quartz-based artificial stone).

added and mixing was continued when the reaction mixture is completely homogenized. The resultant mixture was poured into the mold and high-frequency vibration compaction molding was applied at a frequency of 52.5 Hz, vacuum conditions at 15 mBar, and pressure holding time was 90 seconds. The obtained samples were de-molded, cured in an oven at a temperature of 140 °C for 45 minutes, and allowed to naturally cool to room temperature. Finally, the artificial weathering tests of artificial stone slabs were conducted after cutting with dimensions of 300 × 80 × 20 mm and multi-stage polishing.

## 2.6 Characterizations of UPR and UPR-e-GO composite materials

The surface morphology of e-GO, UPR and UPR/e-GO was investigated using scanning electron microscopy (SEM) (Hitachi S-4000) at an accelerating voltage of 5 kV. The inner structure of UPR/e-GO was analyzed by using a high-resolution transmission electron microscope (HR-TEM) (JEM-2100, Jeol Japan) operated at 200 kV. The hydrodynamic size of e-GO was evaluated *via* dynamic light scattering (DLS) measurement using zetasizer ultra red label equipment. The optical properties of GO, UPR, and UPR/GO were studied by ultraviolet-visible (UV-vis) absorption spectra using a JENWAY 6850 double-beam spectrophotometer. Chemical properties were investigated by Raman spectroscopy using a MacroRAM™ Raman spectrometer (Horiba) with 785 nm laser excitation. The surface property was analyzed by $\zeta$ potential measurements (zetasizer ultra red label). Fourier transform infrared (FTIR) analysis was undertaken using a Spectrum Two, PerkinElmer in the range of 350–8300 cm$^{-1}$. The XRD analysis was performed by using XRD diffractometer (Equinox 5000) with Cu-K$\alpha$ radiation ($\lambda = 1.5406$ Å).

Thermogravimetric analysis (TGA) was conducted on a 4000 PerkinElmer instruments (USA) in the range of 25–700 °C with a heating rate of 10 °C min$^{-1}$ under a nitrogen atmosphere. Differential scanning calorimetry (DSC) was carried out on a DSC8000, PerkinElmer (USA) with a heating rate of 10 °C min$^{-1}$ in flowing N$_2$ from ambient temperature to 200 °C.

The flexural and tensile properties of the UPR/e-GO nanocomposites were carried out using the universal testing machine (Instron 100 kN). Dynamic mechanical properties of the samples were executed using a DMA 8000 (PerkinElmer). The test mode used here was one-point bending with the specimen dimensions being 30 mm × 10 mm × 2 mm. The temperature was set between 30 and 150 °C with a constant heating rate of 4 °C min$^{-1}$ and frequency of 1 Hz.

The artificial weathering test was studied using fluorescent UV/condensation weathering equipment (Atlas UVTest, USA) according to the ASTM G154-06 (2006) standard (standard practice for operating fluorescent light apparatus for UV exposure of nonmetallic materials). The neat UPR and UPR/e-GO specimens were exposed for 1000 hours in intervals of 100 hours and after each interval, the samples were tested. The wavelengths of the UV ray emitted at 340 nm. The cycle consisted of 8 hours of UV radiation with the wavelength of 340 nm at 60 ± 3 °C and 4 hours of condensation at 50 ± 3 °C. The irradiance intensity was 0.89 W m$^{-2}$.

The change in sample color was measured using a benchtop sphere spectrophotometer X-Rite Ci7800 (USA). The change of color $\Delta E$ was calculated by the Euclidean equation:[40]

$$\Delta E = \sqrt{(\Delta L)^2 + (\Delta a)^2 + (\Delta b)^2}$$

where $\Delta L$ represents the brightness relationship between light and dark, $\Delta a$ represents the relationship between green and red, and $\Delta b$ represents the relationship between blue and yellow. The symbol $\Delta$ implies the difference between the samples before and after being aged.

# 3 Results and discussion

## 3.1 Characterizations of functional e-GO nanosheets

The morphology characterization of e-GO nanosheets was observed by using a scan electron microscopy. Fig. 1a shows the SEM image of e-GO nanosheets with wrinkles and folded edges observed. These wrinkle structures may be important for preventing aggregation and boosting dispersion of e-GO nanosheets in the polymer matrix. To estimate the lateral dimensions of e-GO nanosheets, DLS measurement was performed in aqueous medium, and result is shown in Fig. 1b. It can be observed that the hydrodynamic sizes of e-GO nanosheets are mainly distributed in the range from 200 to 600 nm. The optical absorption property of e-GO nanosheets is important for designing the UV-shielding properties to the UPR/e-GO nanocomposites. The UV-vis absorption spectrum of e-GO nanosheets shows a sharp absorption band at 227 nm and a broad shoulder at 302 nm, as shown in Fig. 1c. The absorption bands at 227 nm and 302 nm have been assigned to the $\pi \rightarrow \pi^*$ transition of aromatic C=C bonds and the $n \rightarrow \pi^*$ transition of C=O bond in $sp^3$ hybrid regions, respectively.[41,42] The lattice structure and electronic property of e-GO nanosheets play a critical role in determining the physicochemical attributes of UPR/e-GO nanocomposites. Raman spectroscopy analysis is a powerful technique for exploring the structural properties of

graphene oxide such as number of layers, oxygen content, and defects. The Raman spectrum and multiple Lorentzian peak fit of e-GO nanosheets are displayed in Fig. 1d. The D band occurs at 1330 cm$^{-1}$ arising from the internal structural defects, edge defects, and the disordered regions due to the $sp^3$ hybridized carbon content.[42–44] The G band at 1597 cm$^{-1}$ corresponds to the first-order scattering of the $E_{2g}$ phonon at the Brillouin zone centre.[42–44] The $I_D/I_G$ ratio of e-GO nanosheets is found to be 1.1, suggesting the high defect density of e-GO arising from the $sp^3$ – bonded carbon atoms. Moreover, the average crystalline size of the $sp^2$ domains ($L_a$ nm) was calculated by using Lucchese's equation:[45] $L_a(nm) = (2.4 \times 10^{-10})\lambda^4(I_D/I_G)^{-1}$. Where $\lambda = 785$ nm is wavelength of laser, $L_a$ is the average crystalline size of the $sp^2$ domains. The $L_a$ value for e-GO sample was found to be about 82 nm, suggesting the high integrity of the $sp^2$ graphene sheet (DLS size ~ 400 nm). Thereby, it can be concluded that the disordered regions and the defects mainly arise from the atomic structure at the nanosheets edges. To further clarify structural properties of e-GO nanosheets, Raman spectrum of e-GO nanosheets was deconvoluted using the multiple Lorentzian peak fit. The D* band is found to be around 1098 cm$^{-1}$, which is related to the disordered graphitic lattice of soot provided by the existence of $sp^3$ bonds.[46,47] The D″ band at 1545 cm$^{-1}$ is related to the amorphous phases and crystallinity of sheet.[46] The 2D band located at 2632 cm$^{-1}$ arises from a double-resonance
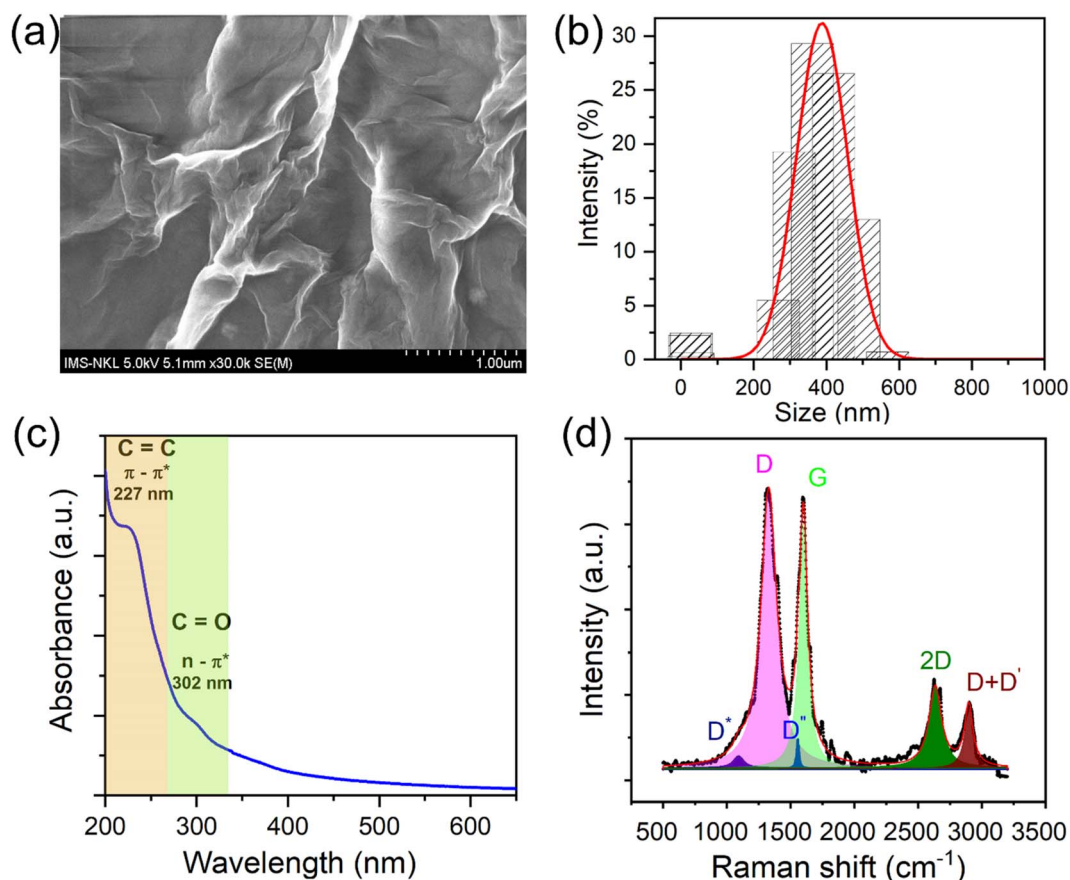


**Fig. 1** SEM image (a); DLS size distribution (b); UV-vis absorption spectrum of e-GO nanosheets (c); Raman spectrum and multiple Lorentzians peak fit of e-GO nanosheets (d).

process, suggesting that the C–C bond concerning sp$^2$ domains remains crystalline with not much strain in between the bonds. Moreover, the $I_{2D}/I_G$ ratio is greatly related to the number of layers of graphene oxide. The $I_{2D}/I_G$ ratio of e-GO nanosheets was calculated to be about 0.35, suggesting that the sample possesses multilayers with layers number over 5 layers.[48] The charge density of the functional groups on the e-GO surface was assessed using ζ potential analysis. The result yielded a significant value of −24.93 mV, even at pH = 3.5, suggesting the formation of a high density of functional groups on the e-GO surface. The obtained analytical results indicate that the e-GO nanosheets not only possess the high defect density, but also retain the integrity of the sp$^2$ graphene sheet. With the above-mentioned excellent features, the as-prepared e-GO nanosheets are expected to be an ideal additive in UPR to enhance its UV-shielding efficiency.

### 3.2 Characterizations of UPR/e-GO nanocomposites

**3.2.1 Morphology of UPR/e-GO materials.** The interfacial interaction of e-GO nanosheets in polymer matrix plays as critical factors for improving the properties of UPR. The morphology and the dispersion behavior of e-GO nanosheets in UPR/e-GO nanocomposites were investigated by SEM observations, as shown in Fig. 2. The SEM image of neat UPR shows a homogeneous surface of polymer film with wrinkles and very few micropore defects (Fig. 2a). For UPR/e-GO nanocomposites (Fig. 2b), only a few marks of e-GO nanosheets can be observed in the homogeneous surface of polymer film, indicating the good dispersion of e-GO nanosheets into the UPR polymer matrix. To elucidate the presence of e-GO within the UPR/e-GO composite, we conducted HR-TEM analysis on this sample (Fig. 2c–f). Fig. 2c highlights that the UPR matrix is nearly
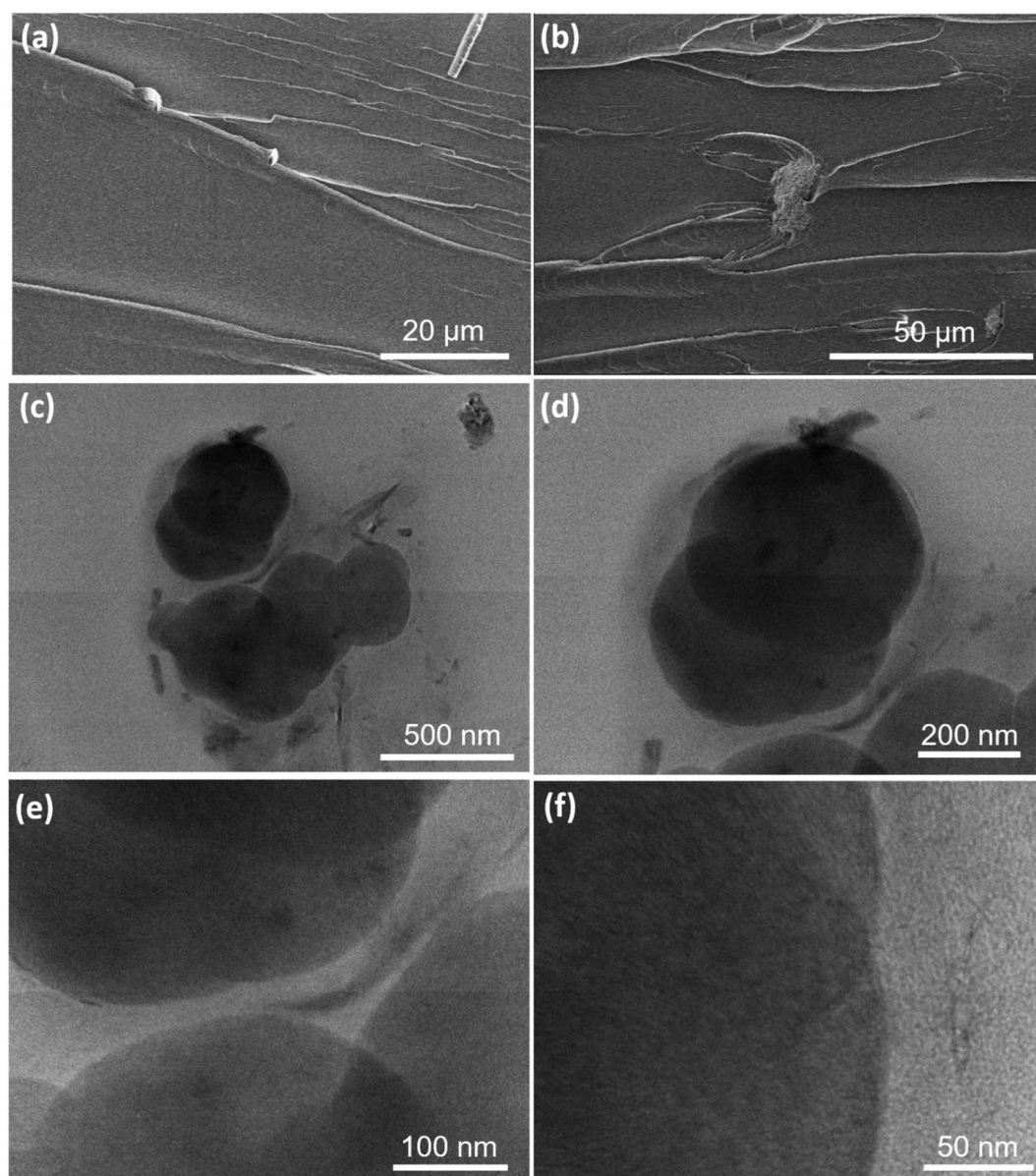


**Fig. 2** SEM images of (a) neat UPR and (b) UPR/e-GO; HR-TEM images of (c–f) UPR/e-GO at different magnifications.

impossible to discern due to its low molecular density and high transmittance, yet the circular sheets of approximately 400–500 nm in diameter stand out clearly. The dimensions of these sheets align with the findings from DLS analysis, which also recorded sizes within the same range, substantiating their identification as e-GO. Higher resolution images (Fig. 2d–f) distinctly highlight the contrast between the boundaries of e-GO sheets and UPR matrix. Taken together, SEM and HR-TEM analyses emphatically demonstrate the successful integration and dispersion of e-GO within the UPR matrix.

### 3.2.2 Structural and chemical properties of UPR/e-GO materials.

Fig. 3a shows the XRD patterns of neat UPR and UPR/e-GO nanocomposites. A broad peak can be observed at approximately $2\theta = 23.43°$ in all the XRD patterns, confirming the amorphous nature of these UPR samples. The XRD patterns of UPR/e-GO nanocomposites are the same as those of the neat UPR, suggesting that the incorporation of e-GO nanosheets does not obviously affect the crystallization characterization of UPR. Moreover, no additional XRD peak associated with GO nanosheets phase was detected, confirming a good dispersion of e-GO nanosheets in UPR polymer matrix.[34,49] Fig. 3b shows the FT-IR spectra of e-GO nanosheets, neat UPR, and UPR/e-GO nanocomposites (0.05 wt%). For e-GO nanosheets, it can be observed two characteristic peaks at 1544 cm$^{-1}$ corresponding to the C=C bonding of aromatic rings of the GO carbon skeleton structure, and 3429 cm$^{-1}$ corresponding to the O–H stretching vibration, respectively.[50] In the FT-IR spectrum of UPR, the peak at 742 cm$^{-1}$ corresponds to the C–H in benzene rings, and the peak at 776 cm$^{-1}$ is assigned to the vibration of $cis$ – CH=CH – bond.[51] Two peaks due to the C=C bonds of polyester chains are found about 980 cm$^{-1}$ and 1640 cm$^{-1}$.[52] The peak at 1066 cm$^{-1}$ can be attributed to the C–O stretching vibration. The peaks at 1255 cm$^{-1}$ and 1118 cm$^{-1}$ originate from the ester linkage C–O–C in UPR molecules.[53,54] The sharp typical band appears at 1719 cm$^{-1}$ corresponding to the C=O stretching vibration in UPR molecules.[55] In addition, multiple peaks in the range of 2900–3100 cm$^{-1}$ are assigned to stretching and rocking of C–H bonds in the alkane.[55] The FT-IR spectrum
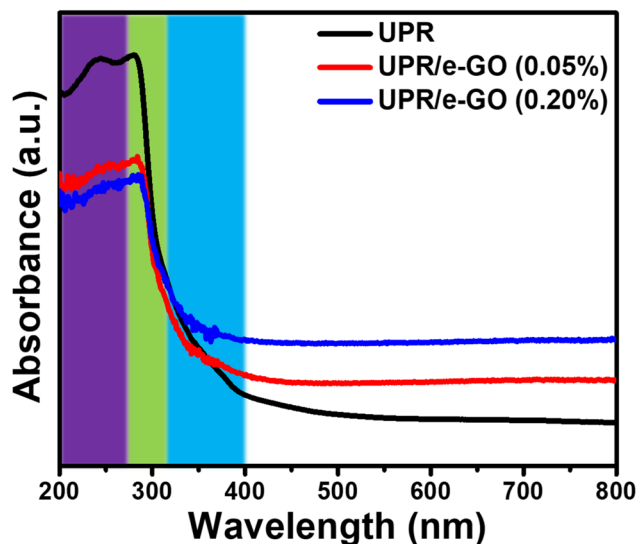


**Fig. 4** UV-vis spectra of neat UPR and UPR/e-GO with different e-GO content.

of UPR/e-GO nanocomposite shows the same feature bands as that of UPR. No obvious change in the intensity and position of main characteristic bands are observed, demonstrating that the dispersion of e-GO nanosheets in the UPR matrix does not impact the bonding features and the formation of UPR.

### 3.2.3 Optical property of UPR/e-GO materials.

Fig. 4 presents the absorption spectra of neat UPR and UPR/e-GO at contents of 0.05 and 0.20 wt%. The neat UPR demonstrates strong UV absorption in the UVC (100–280 nm) and UVB (280–315 nm) ranges, leading to photodegradation that impacts its physical, mechanical, and chemical properties. Because Fig. 1c showed that e-GO possesses efficient UV absorption in these same ranges, the integration of e-GO into the UPR matrix was expected to enhance the UV absorption capability of the UPR/e-GO material. However, contrary to expectations, the incorporation of 0.05 wt% e-GO (red line) resulted in a substantial
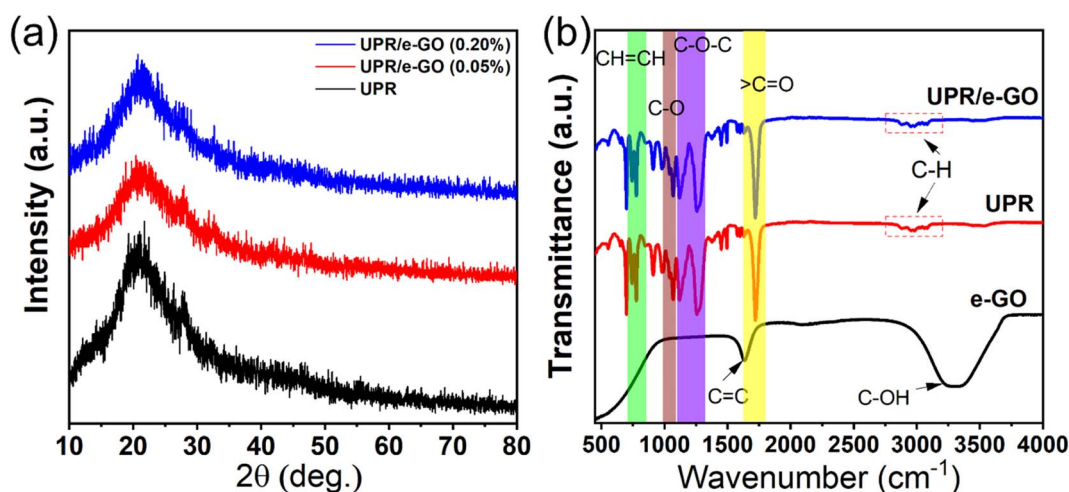


**Fig. 3** XRD pattern of neat UPR and UPR/e-GO (a); FTIR spectra of e-GO, neat UPR and UPR/e-GO (b).

reduction in UV absorption in the UVC and UVB ranges. This downward trend in UV absorption persisted as the e-GO content was increased to 0.20 wt% (blue line). This result suggests that the inclusion of e-GO may decrease the interaction between UV rays and the UPR matrix, potentially acting as a shielding layer that inhibits UPR's direct UV absorption. Furthermore, the UPR/e-GO material exhibits negligible absorption of visible light compared to neat UPR, which aids in maintaining the required transparency of the UPR/e-GO material.

### 3.3 Mechanical property of UPR/e-GO nanocomposite materials

The good dispersion of e-GO nanosheet in the polymer matrix is expected to boost the mechanical properties of UPR/e-GO nanocomposites. To evaluate the reinforcement of e-GO nanosheets on the mechanical properties of UPR/e-GO nanocomposites, flexural and tensile property tests were conducted. Fig. 5 shows the comparisons of flexural and tensile properties for the neat UPR and UPR/e-GO nanocomposites with different e-GO dosages (0.05–0.2 wt%). It can be observed that the UPR/e-GO nanocomposites exhibit the obvious enhancement of flexural and tensile strength in comparison with neat UPR.

Moreover, both flexural and tensile strength increase with the increase of dosage of e-GO nanosheets in the range from 0.05 to 0.2 wt%. The UPR/e-GO nanocomposite sample (0.2 wt%) possesses the flexural strength of 119.5 MPa and tensile strength of 62.6 MPa, which increase by 29% and 32.2% in comparison with the neat UPR, respectively. Flexural modulus and tensile modulus of this sample were found to be about 3.5 GPa and 4.8 GPa, which increase by 17% and 45.7% in comparison with the neat UPR, respectively. The strong interfacial interaction of e-GO nanosheets-polymer matrix can be considered as the direct and intrinsic mechanism contributing to the enhancement of mechanical properties of UPR/e-GO nanocomposites.[56] The e-GO nanosheets with two-dimensional structure play role as a bridge between the polymer chains of UPR through the hydrogen bond and $\pi-\pi$ stacking interaction.[49,56] Then, strong mechanical interlocking would be formed, with polymer chains effectively penetrating the spaces between e-GO nanosheets.[34]

### 3.4 Thermal property of UPR/e-GO nanocomposite materials

The effect of e-GO nanosheets on thermal degradation of UPR resins and UPR/e-GO nanocomposites were studied by TGA
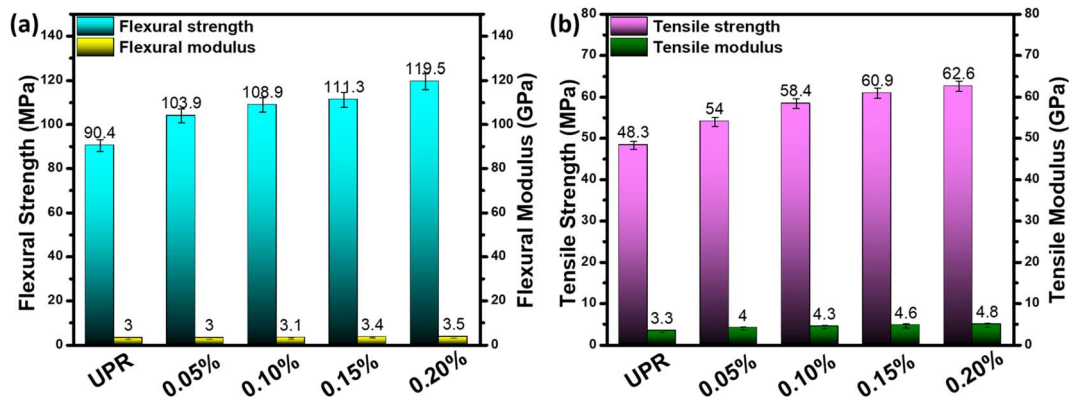


Fig. 5 Flexural (a) and tensile (b) properties of UPR and UPR/e-GO with different e-GO content.
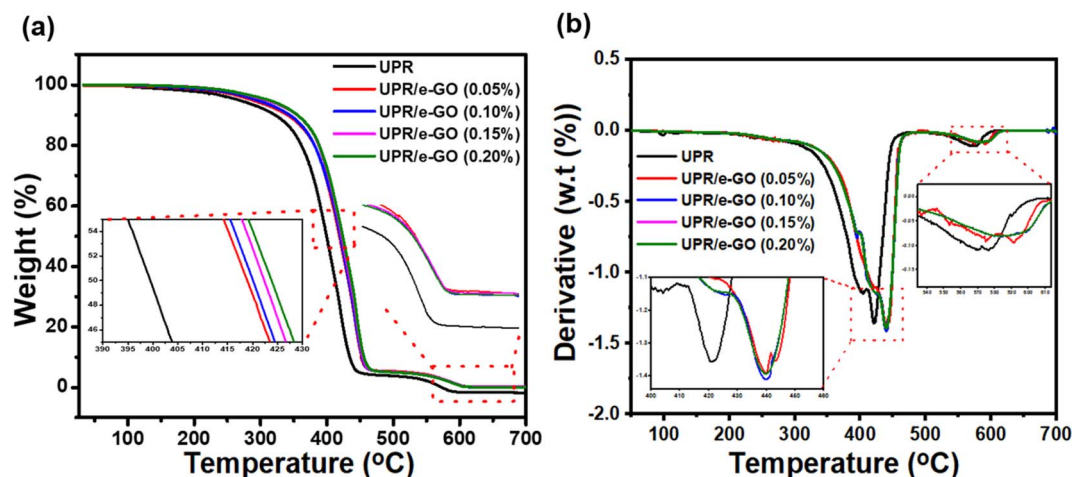


Fig. 6 TGA (a) and DTGA (b) spectra of neat UPR and UPR/e-GO.

**Table 2** The TG and DTG data of the UPR samples under the air condition

| Samples | Temperature (°C) | | | Char residues at 700 °C (wt%) |
|---|---|---|---|---|
| | $T_{10}$ | $T_{50}$ | $T_{1max}/T_{2max}$ | |
| UPR | 322.1 | 399.4 | 419.0/570.6 | 0.00 |
| UPR/e-GO 0.05 wt% | 337.6 | 416.6 | 439.9/591.7 | 0.04 |
| UPR/e-GO 0.10 wt% | 340.6 | 417.7 | 440.0/584.5 | 0.07 |
| UPR/e-GO 0.15 wt% | 351.9 | 419.5 | 439.3/583.9 | 0.14 |
| UPR/e-GO 0.20 wt% | 352.7 | 421.6 | 440.0/584.9 | 0.22 |

method. The TG and DTG results are shown in Fig. 6. Table 2 summarizes the characteristic temperatures of active degradation. The onset degradation temperature of samples which is evaluated by the temperature of 10 wt% weight loss ($T_{10}$), the mid-point temperature of the degradation ($T_{50}$), the fraction of the solid residue material at 700C are obtained from the TG curves, and the temperature of the maximum weight loss rate ($T_{max}$) of samples was obtained from the DTG curve. $T_{1max}$ and $T_{2max}$ are the temperature at the maximum mass lost rate for stage 1 and stage 2, respectively.

As can be seen, the thermal decomposition of the neat UPR starts at 200 °C due to the evaporation of moisture or remaining water, and unreacted monomer. A rapid reduction in weight for neat UPR materials was found with the temperature range from 300 to 450 °C which might be due to the decomposition of polymer chains. The third stage is in a temperature above 450 °C corresponding to the pyrolysis of UPRs in air. The mainly degradable products of this process include unsaturated hydroxyesters, benzaldehydes, phthalic anhydrides, and combustion products such as hydrogen, carbon dioxide, and methane gas.[57,58]

More interestingly, with the inclusion of e-GO nanosheets into UPR matrix, the UPR/e-GO polymer nanocomposites display retardation of thermal degradation. The increased thermal stability of four UPR/e-GO specimens was clearly observed in the shifted degradation temperatures to higher values compared to the neat UPR. The onset decomposition temperature ($T_{10}$) of the polymer chain has been improved and increased with the increasing e-GO content. Introducing higher e-GO content (0.2 wt%) accelerated the thermal stability with the $T_{10}$ and $T_{50}$ values of 352.7 and 421.6 °C compared to 322.1 and 399.4 °C for neat UPR, respectively. The $T_{10}$ and $T_{50}$ values of UPR with 0.2 wt% e-GO improved by 9.5 and 5.6% compared to the pure resin, indicating the UPR specimens modified with e-GO nanosheets were more stable than non-modified UPR specimens. Besides, similar to $T_{10}$ and $T_{50}$ values, the incorporation of e-GO nanosheets showed also slight improvement in the temperature of the maximum weight loss rate ($T_{1max}/T_{2max}$) of UPR/e-GO composites, from 419.0/570.6 °C for neat UPR to 439.9/591.7, 440.0/584.6, 439.3/583.9 and 440.0/584.9 °C for the addition of 0.05, 0.01, 0.15 and 0.2 wt% e-GO, respectively. Furthermore, as the amount of e-GO increases, the char residues at 700 °C increases. The total weight loss for the UPR specimen is 100%, whereas the UPR/e-GO 0.2 wt% specimen shows an ultimate residue of about 0.22% due to the

subsistence of carbon content, revealing the thorough dispersion of the e-GO nanosheets within the UPR polymer matrix.

The substantial increment in thermal stability may be attributed to the strong interaction between UPR and e-GO nanosheets during the *in situ* polycondensation process,[59,60] which leads to a restriction of mobility of polymer molecular chains at the interface between UPR and e-GO nanosheets.[61,62] The interaction can be attributed to dipole interactions and hydrogen bonding between the oxygen-containing functional groups on e-GO and the UPR.[62] The *in situ* formed e-GO nanosheets in the UPR matrix with high aspect ratio and large specific surface area behave like inert filler, acting as barriers to effectively prevent or lower the permeation of oxygen and the escape of volatile degradation products.[34] According to the obtained results, the e-GO nanosheets manifested to be an ideal additive to enhance the thermal stability of the UPR/e-GO polymer nanocomposites even at ultralow levels.

### 3.5 UV resistant efficiency of UPR/e-GO nanocomposites

Influence of UV radiation on the appearance of the neat UPR and UPR/e-GO nanocomposites for different time intervals was also evaluated. The changes in color parameters (*i.e.* $\Delta L$, $\Delta a$, $\Delta b$ and $\Delta E$) of the samples are listened in Table 3. The results show that the neat UPR sample has a value of $\Delta E = 40.03$, exhibiting a visible color change after direct exposure to UV rays. After 1000 hours of UV exposure, the surface of the neat UPR specimen became darker, redder, and yellower. These observations are in good agreement with previously published works.[1,63] Compared to the neat UPR specimen, the lightness index $\Delta L$ of the UPR/e-GO specimen is reduced, implying the presence of e-GO nanosheets in the samples. It can be observed that the $\Delta L$, $\Delta a$, and $\Delta b$ values of four UPR/e-GO specimens are decreased with the increase in the dosage of e-GO nanosheets.

Fig. 7 illustrates the change in color $\Delta E$ as the function of irradiation time for the neat UPR and UPR/e-GO nanocomposites with the different dosage of GO nanosheets into the UPR matrix. As shown in the figure, it is clearly observed that the presence of e-GO nanosheets in the UPR matrix strongly increases the UV resistance of the obtained specimens. As the dosage of e-GO nanosheets increases, the UV resistance also increases. For the UPR/e-GO 0.1 wt%, the $\Delta E$ value (3.43) shows

**Table 3** Three parameters $\Delta L$, $\Delta a$, $\Delta b$ and the change $\Delta E$ of the samples

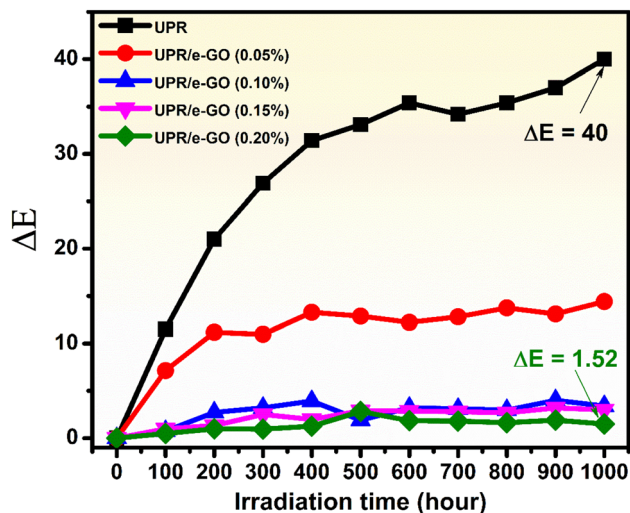| Samples | Irradiation time | $\Delta L$ | $\Delta a$ | $\Delta b$ | $\Delta E$ |
|---|---|---|---|---|---|
| UPR | 0 hour | 93.81 | −1.41 | 4.94 | 0 |
| UPR/e-GO 0.05 wt% | | 48.12 | −0.67 | 6.64 | 0 |
| UPR/e-GO 0.10 wt% | | 28.13 | −0.06 | 1.85 | 0 |
| UPR/e-GO 0.15 wt% | | 25.13 | 0.00 | −0.34 | 0 |
| UPR/e-GO 0.20 wt% | | 26.32 | 0.01 | −0.45 | 0 |
| UPR | 1000 hours | 70.12 | −0.59 | 37.20 | 40.03 |
| UPR/e-GO 0.05 wt% | | 46.27 | 0.91 | 20.86 | 14.42 |
| UPR/e-GO 0.10 wt% | | 30.32 | −0.08 | 4.50 | 3.43 |
| UPR/e-GO 0.15 wt% | | 27.70 | −0.63 | 1.13 | 3.02 |
| UPR/e-GO 0.20 wt% | | 27.43 | −0.49 | 0.47 | 1.52 |

**Fig. 7** The change in $\Delta E$ value over time under UV irradiation of UPR and UPR/e-GO with different e-GO content.

a striking enhancement of UV resistance (increased by 91.5%). In particular, when the concentration of e-GO reached 0.2 wt%, the UV-resistant efficiency was superior to that of neat UPR. The $\Delta E$ value was calculated to be 1.52, which the corresponding UV resistance improvement is 96.5%. From the above results, it can be concluded that the obtained UPR/e-GO nanocomposites can be recognized for their nearly absolute resistance to UV irradiation by combining e-GO nanosheets at proper contents and UPR matrix.

Table 4 reviews various studies that utilized nanomaterials to enhance the mechanical and thermal durability, and UV resistance, of polymers. Specifically, incorporating 4 wt% of 27 nm-sized nano $TiO_2$ into the UPR matrix *via* mechanical stirring markedly improved its mechanical characteristics. Likewise, the $Cu_2O$–$TiO_2$-GO complex (at 2 wt%) boosted fire resistance while significantly reducing toxic emissions during UPR combustion. The $TiO_2@SiO_2$/APTES composite, with its $SiO_2$ shell-diminished photocatalytic properties, aided PPS in elevating UV resistance – evident in the visually perceptible yellowing reduction of PPS sheets under 192 hours of UV exposure, compared to unmodified PPS. Functionalization of GO sheets by maleic anhydride, achieved during the *in situ* polymerization process of the UPR, enhanced its mechanical and thermal durability. However, these studies were limited in their quantitative assessment of UV resistance *via* color change representation and lacked comprehensive evaluation of the enhanced mechanical, thermal, and UV-shielding properties. Our research quantitatively evaluated and demonstrated an excellent enhancement in UV-shielding (96% – nearly complete) when using e-GO nanosheets, and provided a comprehensive evaluation of enhanced mechanical properties and thermal retardancy.

### 3.6 Discussion of enhanced UV resistant mechanism of UPR/e-GO composite materials

To elucidate the effect of e-GO nanosheets on the UPR properties and provide detailed information regarding the interface interaction in the nanocomposites, we carried out dynamic

**Table 4** Comparing the improvement in mechanical, thermal, and UV-shielding properties of several nano-modified polymers. (Poly(urethane acrylate) (PUA), polyphenylene sulfide (PPS), graphene (GE), functionalized-graphene oxide (f-GO))

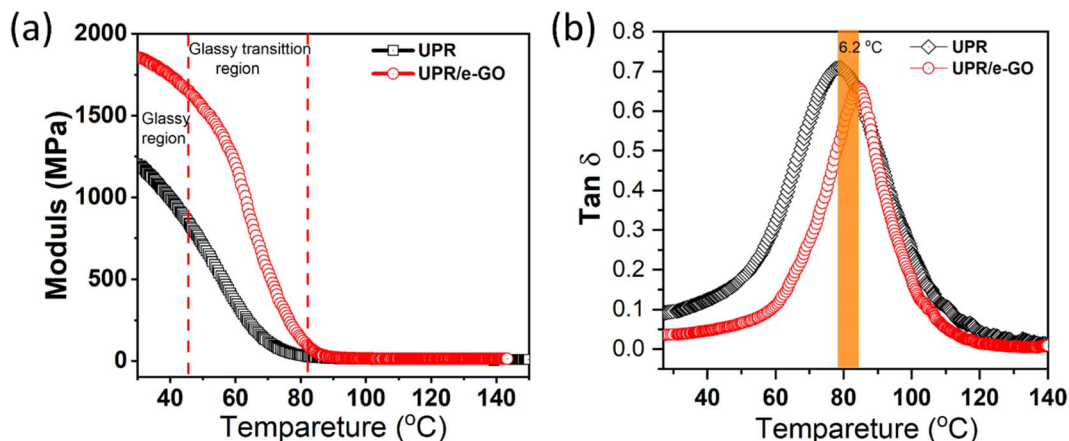| Materials | Synthesized method | Mechanical enhancement (%) | Thermal enhancement (%) | UV-shielding enhancement | Ref. |
|---|---|---|---|---|---|
| UPR/TiO₂ (4 wt%) | Mechanical stirring | Tensile strength (47%) Bending strength (173%) Impact strength (60%) | — | — | 64 |
| PUA/ZnO (0.3 wt%) | Ultrasonic dispersion | - Tensile strength (56%) Young's modulus (53%) | — | Potential application due to increasing UV absorbance | 65 |
| PPS/TiO₂@SiO₂/ APTES (1 wt%) | Mechanical stirring | Breaking strength retention rates (38%) Breaking elongation retention rates (39%) | — | Reducing the yellowing of the PPS sheet after 192 hours of UV radiation exposure | 66 |
| UPR/Cu₂O–TiO₂-GO (2 wt%) | Ultrasonic dispersion | — | Enhancing fire resistance while significantly decreasing toxic emissions during combustion | — | 37 |
| UPR/GE (1.5 wt%) | — | Hardness (11%) Flexural strength (39%) Tensile strength (115%) | Tg (26%) | — | 36 |
| UPR/f-GO (0.04 wt%) | *In situ* polymerization | Tensile strength (75%) Storage modulus (54%) | $T_{10}$ (27%) | — | 38 |
| UPR/e-GO (0.2 wt%) | *In situ* polymerization | Flexural strength (32%) Tensile strength (28%) Tensile strength (28%) Tensile modulus (46%) | $T_{10}$ (9%) $T_{50}$ (5%) To (14%) | 96% (nearly complete UV-shielding) | This work |

**Fig. 8** Dynamic mechanical thermal analysis (DMA) spectra: (a) storage modulus ($E'$) and (b) loss factor (tan $\delta$) of UPR and UPR/e–GO.

mechanical thermal (DMA) analysis.[67] The results of DMA experiments on the UPR and UPR/e-GO samples are represented in Fig. 8. As can be observed in Fig. 8a, storage modulus ($E'$) of neat UPR is found to be 995 MPa at 40 °C. After incorporation e-GO nanosheets into UPR matrix, the storage modulus ($E'$) reaches 1706 MPa, increases by 71.4% in comparison with neat UPR. Moreover, $E'$ is enhanced at all the temperatures in the range of 40–90 °C, confirming that the UPR matrix is effectively reinforced by e-GO nanosheets, similar to the obtained results from the flexural and tensile tests. The enhancement in storage modulus of UPR/e-GO nanocomposites can be attributed due to the fine dispersion and strong interfacial interaction of e-GO nanosheet with polymer chains.[68] In addition, the glass transition temperature ($T_g$) of neat UPR and UPR/e-GO nanocomposites were found to be about 78.3 °C and 84.5 °C, respectively. It was indicated that the value of $T_g$ increases with increasing in the cross-linking density of UPR-based composites.[67,68]

The loss factor (tan $\delta$) is the ratio of loss modulus ($E''$) and storage modulus ($E'$). Fig. 8b shows the evolution of tan $\delta$ with the temperature for neat UPR and UPR/e-GO nanocomposites (0.20 wt%). It can be observed that the peak of tan $\delta$ is shifted to the higher temperature with incorporation e-GO nanosheets into UPR matrix. Besides, the tan $\delta$ peak height for UPR/e-GO nanocomposites is calculated about 0.65, significantly lower than that of neat UPR (0.71), implying that the molecule mobility of polyester chains decreases after interaction with e-GO nanosheets.[69] Obviously, the UPR/e-GO nanocomposites possess a higher $E'$ value with lower tan $\delta$ value than those of neat UPR, confirming the strong interfacial bond between e-GO nanosheets and polymer chains. This strong interfacial interaction can be attributed to strong hydrogen bonding and crosslinking between oxygen-containing functional groups of GO and polymer chains of UPR.

Many previous studies have demonstrated that the formation of free radicals is one of the primary causes of the photodegradation of UPR polymer exposed to UV radiation.[7,14–18] These active intermediates can trigger off chain scission, crosslinking, branching, and rearrangement in UPR molecular,

resulting the fragmentation and destruction of UPR chains.[7,17,18] The application of semiconductor nanoparticles, such as ZnO and TiO$_2$, has been a strategy for shielding the UPR chain from UV rays.[37,64,65] These materials capitalize on their high UV absorption properties and their capacity for direct interaction with polymer chains, thanks to their nanoscale size. Nonetheless, the high photocatalytic activity of these semiconductors poses a significant limitation, as it unintentionally induces polymer chain degradation.[66] A potential solution to this issue involves encasing the semiconductor nanoparticles in an insulator such as SiO$_2$ to diminish their photocatalytic activity.[70] This method has shown encouraging results, yet it complicates the synthesized material process. Consequently, nano GO material has emerged as a promising alternative, given its superior UV absorption capabilities and virtually non-existent photocatalytic activity. The UV-vis absorption spectra confirm that the incorporation of e-GO into UPR/e-GO lessens the overall UV absorption. Furthermore, SEM and HR-TEM imaging confirm the uniform dispersion of e-GO within the UPR network. The excellent UV-resistant behavior of the UPR/e-GO nanocomposites could be explained in the following way. (1) e-GO possess a strong UV absorptance thanks to the presence of a conjugated aromatic structure (see UV-vis results in Section 3.1).[70] The overall decrease in the UV absorption intensity of the sample can be explained by the presence of e-GO sheets in the UPR matrix. These sheets serve a dual function – they absorb UV rays and act as a protective barrier, mitigating UV interactions with the UPR base resin. A crucial aspect contributing to this comprehensive protection is the homogeneous dispersion and absence of aggregation, ensuring that protection is homogeneous throughout the sample. After the UV absorption process, the e-GO nanosheets dissipated UV radiation *via* converting the absorbed radiation energy into heat to prevent the damaging UV-rays.[71] (2) Another mechanism for UV-resistance of UPR/e-GO nanocomposites is the role of e-GO nanosheets in scattering the UV rays.[72] The e-GO nanosheets can reflect UV-rays because of the unique planar 2D structure.[70] The observed decrease in the overall UV absorption of UPR/e-GO could stem from the UV reflection process, which in turn inhibits UV rays
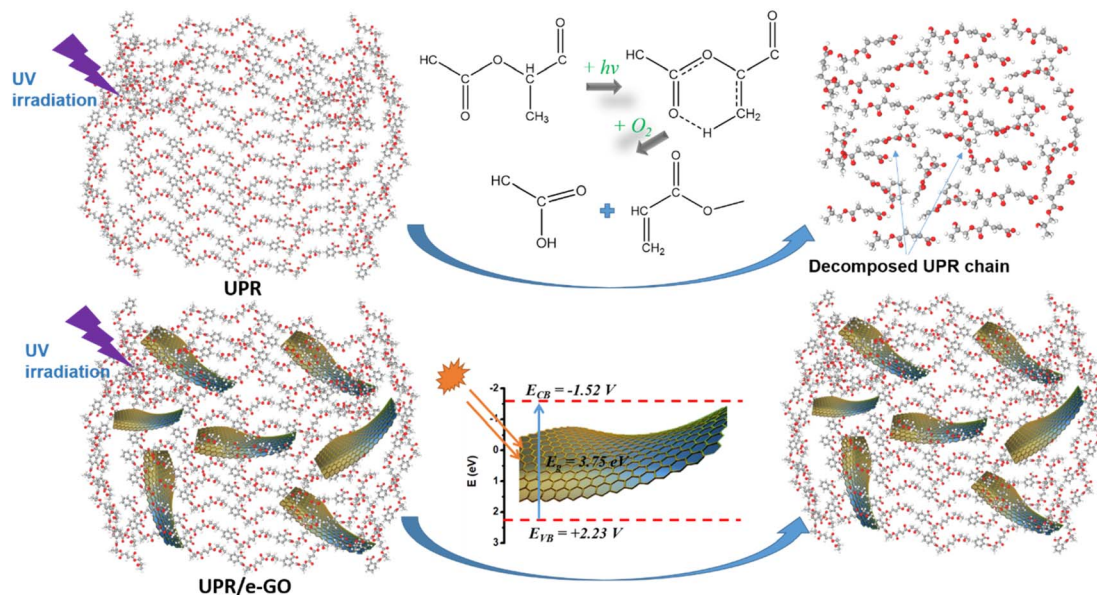
**Fig. 9** Possible mechanism of enhancement UV resistance in UPR/e-GO nanocomposites compared to neat UPR.

from interacting with the UPR chain, thereby preventing the onset of the aging process. (3) The thin film structure of e-GO provides a significantly larger protective area against UV rays compared to nanoparticle structures. This attribute is another pivotal factor driving the total outstanding UV resistance of the UPR/e-GO material. The possible mechanism of enhancement UV resistance in UPR/e-GO nanocomposites was presented in Fig. 9. In summary, the incorporation of e-GO nanosheets not only merely improved the mechanical performance of UPR composites but also significantly enhanced the UV resistance, contributing to the development of outdoor applications of this valuable resin and elongate their lifetime.

### 3.7 Application of UPR/e-GO composite materials in artificial quartz stone samples and their UV resistant durability

Artificial quartz stone product is a composite material that has seen widespread use in many applications due to various advantages coming from ultra-high hardness, high chemical stability, and easy cleaning. However, deterioration factors such as temperature, moisture, and ultraviolet radiation (UV) may limit the outdoor applications of the products. UPR only accounts for 10% of the product, but this is the main cause of color change of artificial stone products. Fig. 10a shows the
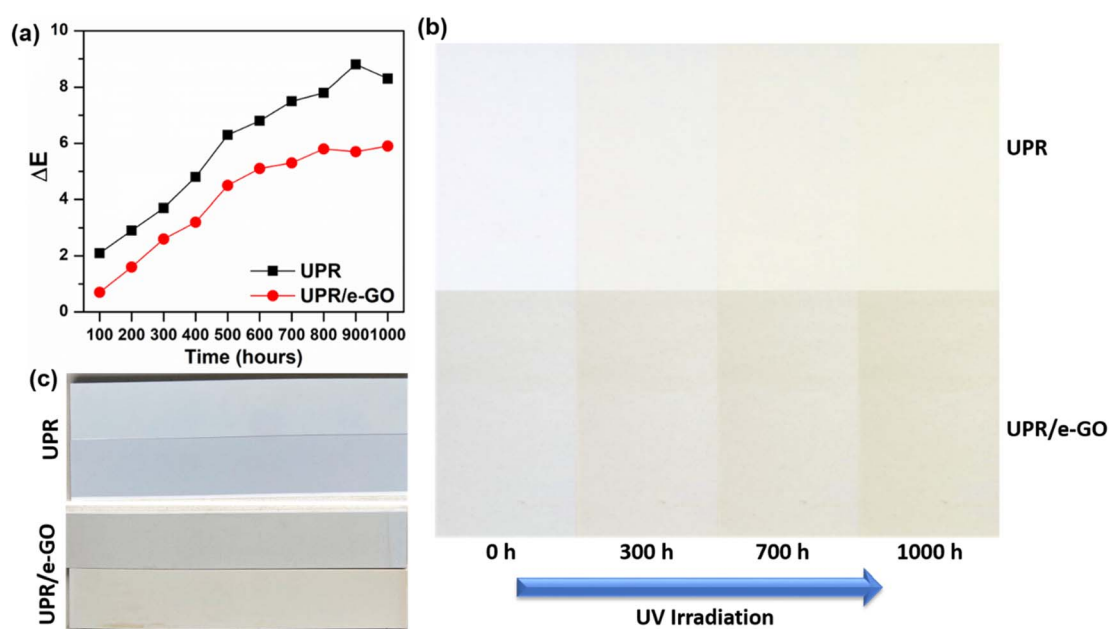


**Fig. 10** Color change of materials after UV irradiation when measuring color (a) and artificial quartz stone samples (b and c).

changes in the $\Delta E$ values of the artificial stone specimens using neat UPR and UPR/e-GO nanocomposites at different aging times in the UV weathering test. For the artificial stone slab using neat UPR, the obtained $\Delta E$ value of 8.3 shows a relatively high level of color variation. Meanwhile, after 1000 hours of UV irradiation, the UPR/e-GO-based artificial quartz stone showed a marked decrease in $\Delta E$ value up to 30% ($\Delta E = 5.9$) compared to the neat UPR-based artificial quartz stone. The enhancement effect of UV resistance in UPR/e-GO-based artificial quartz stone has also been demonstrated through images of stone samples before and after UV irradiation (Fig. 10b). For the specimen using the neat UPR, the yellowing and darkening phenomena occurring upon UV irradiation. When observing the artificial stone using UPR/e-GO, the specimen showed a slight change, yellowing but the variation was lower than that of the artificial quartz stone specimen using neat UPR. Therefore, with enhanced UV-resistant properties, the as-prepared UPR/e-GO polymer nanocomposites are well suited to outdoor applications of artificial stone products.

## 4. Conclusions

In summary, the UPR/e-GO polymer nanocomposites were successfully prepared by incorporating the electrochemically exfoliated GO nanosheets into the UPR matrix *via in situ* polymerization approach. The mechanical properties, thermal stability, and anti-UV aging performance of UPR/e-GO nanocomposites containing different ultra-low e-GO contents of 0.05, 0.1, 0.15, and 0.2 wt% were investigated. The results showed that the inclusion of e-GO nanosheets into UPR enabled the comprehensive property enhancement of the UPR/e-GO nanocomposites. The flexural strength, flexural modulus, tensile strength, tensile modulus of the UPR/e-GO 0.2 wt% specimen are 119.5 MPa, 3.5 GPa, 62.6 MPa, and 4.8 GPa, respectively, which increase by 32.2%, 17.0%, 27.7%, and 45.7% compared to the neat UPR, respectively. The $T_{10}$ and $T_{50}$ decomposition temperatures were increased by 30.6 and 22.3°, respectively, despite the addition of e-GO as low as 0.2 wt%. The DMA results also showed that the $T_g$ and $E'$ values of the UPR/e-GO 0.2 wt% specimen increased by 14.1% and 71.4%, respectively, while the tan $\delta$ values decreased from 0.71 to 0.65 when compared to the neat UPR. Furthermore, using e-GO nanosheets with controlled weight contents of 0.2 wt% can improve the UV resistance by more than 96%. The possible mechanism of enhancement UV resistance in UPR/e-GO nanocomposites was discussed in detail. The results of practical application in artificial stone and UV-resistant durability have shown that the UPR/e-GO nanocomposite holds great potential for manufacturing quartz-based engineered stones for both indoor and outdoor applications.

## Author contributions

N. A. Son: conceptualization, methodology, validation, investigation, writing – original draft; D. Q. Thuc: conceptualization, methodology, validation, formal analysis, writing – original draft; Q. D. Mai: conceptualization, methodology, validation, formal analysis, writing – original draft; N. H. Nguyen: validation, formal analysis, writing – review & editing; N. T. Anh: validation, formal analysis, writing – review & editing; N. X. Dinh: validation, formal analysis, writing – review & editing; P. A. Tuan: conceptualization, methodology, supervision, project administration, writing – review & editing; A. T. Le: conceptualization, methodology, supervision, project administration, writing – review & editing.

## Conflicts of interest

The authors declare that they have no known competing financial interests or personal relationships that could have appeared to influence the work reported in this paper.

## Acknowledgements

## References

1 Z. Jia, X. Li and Q. Zhao, Effect of artificial weathering on surface properties of unsaturated polyester (UP) resin, *Mater. Chem. Phys.*, 2010, **121**, 193–197.

2 S. Marais, F. Gouanvé, A. Bonnesoeur, J. Grenet, F. Poncin-Epaillard, C. Morvan and M. Métayer, Unsaturated polyester composites reinforced with flax fibers: effect of cold plasma and autoclave treatments on mechanical and permeation properties, *Composites, Part A*, 2005, **36**, 975–986.

3 M. Malik, V. Choudhary and I. K. Varma, Current status of unsaturated polyester resins, *J. Macromol. Sci. Part C*, 2000, **40**, 139–165.

4 B. Dholakiya, Unsaturated polyester resin for specialty applications, *Polyester*, 2012, **7**, 167–202.

5 E. Kicko-Walczak and G. Rymarz, Flame-retardant unsaturated polyester resins: an overview of past and recent developments, *Polyester—Prod., Charact. Innov. Appl.*, 2018, 21–44.

6 D. K. Rajak, D. D. Pagar, P. L. Menezes and E. Linul, Fiber-reinforced polymer composites: manufacturing, properties, and applications, *Polymers*, 2019, **11**, 1667.

7 A. Kandelbauer, G. Tondi, O. C. Zaske, and S. H. Goodman, Unsaturated polyesters and vinyl esters, in *Handb. Thermoset Plast.*, Elsevier, 2022, pp. 97–158.

8 J. Pospíšil, J. Pilař, N. C. Billingham, A. Marek, Z. Horak and S. Nešpůrek, Factors affecting accelerated testing of polymer photostability, *Polym. Degrad. Stab.*, 2006, **91**, 417–422.

9 N. M. Ainali, D. N. Bikiaris and D. A. Lambropoulou, Aging effects on low-and high-density polyethylene, polypropylene and polystyrene under UV irradiation: an insight into decomposition mechanism by Py-GC/MS for

microplastic analysis, *J. Anal. Appl. Pyrolysis*, 2021, **158**, 105207.

10  J. Qin, J. Jiang, Y. Tao, S. Zhao, W. Zeng, Y. Shi, T. Lu, L. Guo, S. Wang and X. Zhang, Sunlight tracking and concentrating accelerated weathering test applied in weatherability evaluation and service life prediction of polymeric materials: a review, *Polym. Test.*, 2021, **93**, 106940.

11  E. Yousif and R. Haddad, Photodegradation and photostabilization of polymers, especially polystyrene, *Springerplus*, 2013, **2**, 1–32.

12  D. Feldman, Polymer weathering: photo-oxidation, *J. Polym. Environ.*, 2002, **10**, 163–173.

13  B. Singh and N. Sharma, Mechanistic implications of plastic degradation, *Polym. Degrad. Stab.*, 2008, **93**, 561–584.

14  N. Miskolczi, Polyester resins as a matrix material in advanced fibre-reinforced polymer (FRP) composites, in *Adv. Fibre-Reinforced Polym. Compos. Struct. Appl.*, Elsevier, 2013, pp. 44–68.

15  Y. C. Ching, T. M. S. U. Gunathilake, K. Y. Ching, C. H. Chuah, V. Sandu, R. Singh and N.-S. Liou, Effects of high temperature and ultraviolet radiation on polymer composites, in *Durab. Life Predict. Biocomposites, Fibre-Reinforced Compos. Hybrid Compos.*, Elsevier, 2019, pp. 407–426.

16  M. T. Rahman, M. A. Hoque, G. T. Rahman, M. M. Azmi, M. A. Gafur, R. A. Khan and M. K. Hossain, $Fe_2O_3$ nanoparticles dispersed unsaturated polyester resin based nanocomposites: effect of gamma radiation on mechanical properties, *Radiat. Eff. Defects Solids*, 2019, **174**, 480–493.

17  K. Chrissafis and D. Bikiaris, Can nanoparticles really enhance thermal stability of polymers? Part I: an overview on thermal decomposition of addition polymers, *Thermochim. Acta*, 2011, **523**, 1–24.

18  H. Kaczmarek, Changes to polymer morphology caused by UV irradiation: 1. Surface damage, *Polymer*, 1996, **37**, 189–194.

19  S. K. Nemani, R. K. Annavarapu, B. Mohammadian, A. Raiyan, J. Heil, M. A. Haque, A. Abdelaal and H. Sojoudi, Surface modification of polymers: methods and applications, *Adv. Mater. Interfaces*, 2018, **5**, 1801247.

20  N. Karak, Fundamentals of nanomaterials and polymer nanocomposites, in *Nanomater. Polym. Nanocomposites*, Elsevier, 2019, pp. 1–45.

21  R. Krishnamoorti and R. A. Vaia, Polymer nanocomposites, *J. Polym. Sci., Part B: Polym. Phys.*, 2007, **45**, 3252–3256.

22  J. Jancar, J. F. Douglas, F. W. Starr, S. K. Kumar, P. Cassagnau, A. J. Lesser, S. S. Sternstein and M. J. Buehler, Current issues in research on structure–property relationships in polymer nanocomposites, *Polymer*, 2010, **51**, 3321–3343.

23  H. Wu, W. P. Fahy, S. Kim, H. Kim, N. Zhao, L. Pilato, A. Kafi, S. Bateman and J. H. Koo, Recent developments in polymers/polymer nanocomposites for additive manufacturing, *Prog. Mater. Sci.*, 2020, **111**, 100638.

24  S. Yuan, F. Shen, C. K. Chua and K. Zhou, Polymeric composites for powder-based additive manufacturing: materials and applications, *Prog. Polym. Sci.*, 2019, **91**, 141–168.

25  H. Chen, X. Tian and J. Liu, Unsaturated polyester resin nanocomposites containing ZnO modified with oleic acid activated by *N,N'*-carbonyldiimidazole, *Polymers*, 2018, **10**, 362.

26  G. Peng, Q. Li, Y. Yang and H. Wang, Degradation of nano ZnO-glass fiber-unsaturated polyester composites, *J. Appl. Polym. Sci.*, 2009, **114**, 2128–2133.

27  M. T. Rahman, M. A. Hoque, G. T. Rahman, M. A. Gafur, R. A. Khan and M. K. Hossain, Study on the mechanical, electrical and optical properties of metal-oxide nanoparticles dispersed unsaturated polyester resin nanocomposites, *Results Phys*, 2019, **13**, 102264.

28  S. Dadashi-Silab, M. Atilla Tasdelen, A. Mohamed Asiri, S. Bahadar Khan and Y. Yagci, Photoinduced atom transfer radical polymerization using semiconductor nanoparticles, *Macromol. Rapid Commun.*, 2014, **35**, 454–459.

29  C. Mendes-Felipe, J. Oliveira, I. Etxebarria, J. L. Vilas-Vilela and S. Lanceros-Mendez, State-of-the-art and future challenges of UV curable polymer-based smart materials for printing technologies, *Adv. Mater. Technol.*, 2019, **4**, 1800618.

30  Q. Xiang, J. Yu and M. Jaroniec, Graphene-based semiconductor photocatalysts, *Chem. Soc. Rev.*, 2012, **41**, 782–796.

31  J. A. Menéndez, A. Arenillas, B. Fidalgo, Y. Fernández, L. Zubizarreta, E. G. Calvo and J. M. Bermúdez, Microwave heating processes involving carbon materials, *Fuel Process. Technol.*, 2010, **91**, 1–8.

32  A. C. M. de Moraes, P. F. Andrade, A. F. de Faria, M. B. Simões, F. C. C. S. Salomão, E. B. Barros, M. do Carmo Gonçalves and O. L. Alves, Fabrication of transparent and ultraviolet shielding composite films based on graphene oxide and cellulose acetate, *Carbohydr. Polym.*, 2015, **123**, 217–227.

33  K. P. Loh, Q. Bao, G. Eda and M. Chhowalla, Graphene oxide as a chemically tunable platform for optical applications, *Nat. Chem.*, 2010, **2**, 1015–1024.

34  C. Bora, P. Gogoi, S. Baglari and S. K. Dolui, Preparation of polyester resin/graphene oxide nanocomposite with improved mechanical strength, *J. Appl. Polym. Sci.*, 2013, **129**, 3432–3438.

35  X. Yang, S. Shang and L. Li, Layer-structured poly (vinyl alcohol)/graphene oxide nanocomposites with improved thermal and mechanical properties, *J. Appl. Polym. Sci.*, 2011, **120**, 1355–1360.

36  H. G. Attiya, T. M. Al-Saadi and A. W. Watan, Preparation and study of the mechanical properties of unsaturated polyester resin/graphene nanocomposite, in *Solid State Phenom.*, Trans Tech Publ, 2019, pp. 83–90.

37  D. Wang, Y. Kan, X. Yu, J. Liu, L. Song and Y. Hu, *In situ* loading ultra-small $Cu_2O$ nanoparticles on 2D hierarchical $TiO_2$-graphene oxide dual-nanosheets: towards reducing fire hazards of unsaturated polyester resin, *J. Hazard. Mater.*, 2016, **320**, 504–512.

38 N. Divakaran, X. Zhang, M. B. Kale, T. Senthil, S. Mubarak, D. Dhamodharan, L. Wu and J. Wang, Fabrication of surface modified graphene oxide/unsaturated polyester nanocomposites *via in situ* polymerization: comprehensive property enhancement, *Appl. Surf. Sci.*, 2020, **502**, 144164.

39 D. T. N. Nga, N. L. N. Trang, V.-T. Hoang, X.-D. Ngo, P. T. Nhung, D. Q. Tri, N. D. Cuong, P. A. Tuan, T. Q. Huy and A.-T. Le, Elucidating the roles of oxygen functional groups and defect density of electrochemically exfoliated GO on the kinetic parameters towards furazolidone detection, *RSC Adv.*, 2022, **12**, 27855–27867.

40 W. S. Mokrzycki and M. Tatol, Colour difference∆ E-A survey, *Mach. Graph. Vis.*, 2011, **20**, 383–411.

41 J. I. Paredes, S. Villar-Rodil, A. Martínez-Alonso and J. M. D. Tascón, Graphene oxide dispersions in organic solvents, *Langmuir*, 2008, **24**, 10560–10564, DOI: **10.1021/la801744a**.

42 S. Saxena, T. A. Tyson, S. Shukla, E. Negusse, H. Chen and J. Bai, Investigation of structural and electronic properties of graphene oxide, *Appl. Phys. Lett.*, 2011, **99**, 013104, DOI: **10.1063/1.3607305**.

43 R. J. Nemanich, G. Lucovsky and S. A. Solin, Infrared active optical vibrations of graphite, *Solid State Commun.*, 1977, **23**, 117–120, DOI: **10.1016/0038-1098(77)90663-9**.

44 K. N. Kudin, B. Ozbas, H. C. Schniepp, R. K. Prud'homme, I. A. Aksay and R. Car, Raman spectra of graphite oxide and functionalized graphene sheets, *Nano Lett.*, 2008, **8**, 36–41, DOI: **10.1021/nl071822y**.

45 M. M. Lucchese, F. Stavale, E. H. M. Ferreira, C. Vilani, M. V. O. Moutinho, R. B. Capaz, C. A. Achete and A. Jorio, Quantifying ion-induced defects and Raman relaxation length in graphene, *Carbon*, 2010, **48**, 1592–1597, DOI: **10.1016/j.carbon.2009.12.057**.

46 S. Claramunt, A. Varea, D. López-Díaz, M. M. Velázquez, A. Cornet and A. Cirera, The importance of interbands on the interpretation of the raman spectrum of graphene oxide, *J. Phys. Chem. C*, 2015, **119**, 10123–10129, DOI: **10.1021/acs.jpcc.5b01590**.

47 D. López-Díaz, M. López Holgado, J. L. García-Fierro and M. M. Velázquez, Evolution of the Raman spectrum with the chemical composition of graphene oxide, *J. Phys. Chem. C*, 2017, **121**, 20489–20497, DOI: **10.1021/acs.jpcc.7b06236**.

48 J.-B. Wu, M.-L. Lin, X. Cong, H.-N. Liu and P.-H. Tan, Raman spectroscopy of graphene-based materials and its applications in related devices, *Chem. Soc. Rev.*, 2018, **47**, 1822–1873, DOI: **10.1039/C6CS00915H**.

49 W. Cai, X. Feng, W. Hu, Y. Pan, Y. Hu and X. Gong, Functionalized graphene from electrochemical exfoliation for thermoplastic polyurethane: thermal stability, mechanical properties, and flame retardancy, *Ind. Eng. Chem. Res.*, 2016, **55**, 10681–10689, DOI: **10.1021/acs.iecr.6b02579**.

50 S. W. Chook, C. H. Chia, S. Zakaria, M. K. Ayob, K. L. Chee, N. M. Huang, H. M. Neoh, H. N. Lim, R. Jamal and R. M. F. R. A. Rahman, Antibacterial performance of Ag nanoparticles and AgGO nanocomposites prepared *via*

rapid microwave-assisted synthesis method, *Nanoscale Res. Lett.*, 2012, **7**, 541, DOI: **10.1186/1556-276X-7-541**.

51 J. Lucki, J. F. Rabek, B. Rånby and C. Ekström, Photolysis of polyesters, *Eur. Polym. J.*, 1981, **17**, 919–933, DOI: **10.1016/0014-3057(81)90198-1**.

52 C. M. C. Pereira, M. Herrero, F. M. Labajos, A. T. Marques and V. Rives, Preparation and properties of new flame retardant unsaturated polyester nanocomposites based on layered double hydroxides, *Polym. Degrad. Stab.*, 2009, **94**, 939–946, DOI: **10.1016/j.polymdegradstab.2009.03.009**.

53 F. Chu, X. Zhou, X. Mu, Y. Zhu, W. Cai, Y. Zhou, Z. Xu, B. Zou, Z. Mi and W. Hu, An insight into pyrolysis and flame retardant mechanism of unsaturated polyester resin with different valance states of phosphorus structures, *Polym. Degrad. Stab.*, 2022, **202**, 110026, DOI: **10.1016/j.polymdegradstab.2022.110026**.

54 F. Chu, D. Zhang, Y. Hou, S. Qiu, J. Wang, W. Hu and L. Song, Construction of hierarchical natural fabric surface structure based on two-dimensional boron nitride nanosheets and its application for preparing biobased toughened unsaturated polyester resin composites, *ACS Appl. Mater. Interfaces*, 2018, **10**, 40168–40179, DOI: **10.1021/acsami.8b15355**.

55 A. K. M. Moshiul Alam, M. D. H. Beg, R. M. Yunus, M. Bijarimi, M. F. Mina, K. H. Maria and T. Mieno, Modification of structure and properties of well-dispersed dendrimer coated multi-walled carbon nanotube reinforced polyester nanocomposites, *Polym. Test.*, 2018, **68**, 116–125, DOI: **10.1016/j.polymertesting.2018.04.005**.

56 J. Wang, X. Jin, C. Li, W. Wang, H. Wu and S. Guo, Graphene and graphene derivatives toughening polymers: Toward high toughness and strength, *Chem. Eng. J.*, 2019, **370**, 831–854, DOI: **10.1016/j.cej.2019.03.229**.

57 G. S. Learmonth and A. Nesbit, Flammability of polymers. v. thermal volatilisation analysis of polyester resin compositions, *Br. Polym. J.*, 1972, **4**, 317–325.

58 N. X. Ho, T. A. Pham, H. T. Ha, T. Q. Dong, N. H. Nguyen and D. V. Tran, Enhancement of UV resistance and thermal stability of the unsaturated polyester material by introducing MHHPA fragment into the molecular skeleton, in *Proc. 2nd Annu. Int. Conf. Mater. Mach. Methods Sustain. Dev.*, Springer, 2021, pp. 428–436.

59 C. Liu, Z. Wang, H. Xie, Z. Liu, Y. Chen, W. Lei, L. Hu, Y. Zhou and R. Cheng, One-pot preparation of unsaturated polyester nanocomposites containing functionalized graphene sheets *via* a novel solvent-exchange method, *RSC Adv.*, 2013, **3**, 22380–22388.

60 H. Saleem, A. Edathil, T. Ncube, J. Pokhrel, S. Khoori, A. Abraham and V. Mittal, Mechanical and thermal properties of thermoset–graphene nanocomposites, *Macromol. Mater. Eng.*, 2016, **301**, 231–259.

61 Y. Zhang, Q. Zhang, D. Hou and J. Zhang, Tuning interfacial structure and mechanical properties of graphene oxide sheets/polymer nanocomposites by controlling functional groups of polymer, *Appl. Surf. Sci.*, 2020, **504**, 144152.

62 P. A. Small, Some factors affecting the solubility of polymers, *J. Appl. Chem.*, 1953, **3**, 71–80.

63 U. Müller, M. Rätzsch, M. Schwanninger, M. Steiner and H. Zöbl, Yellowing and IR-changes of spruce wood as result of UV-irradiation, *J. Photochem. Photobiol. B Biol.*, 2003, **69**, 97–105.

64 X. Yinghong, W. Xin, Y. Xujie and L. Lude, Nanometre-sized $TiO_2$ as applied to the modification of unsaturated polyester resin, *Mater. Chem. Phys.*, 2003, **77**, 609–611.

65 S. Zhang, D. Zhang, H. Bai and W. Ming, ZnO nanoparticles coated with amphiphilic polyurethane for transparent polyurethane nanocomposites with enhanced mechanical and UV-shielding performance, *ACS Appl. Nano Mater.*, 2019, **3**, 59–67.

66 Y. Bai, Z. Li, B. Cheng, M. Zhang and K. Su, Higher UV-shielding ability and lower photocatalytic activity of TiO 2@ SiO$_2$/APTES and its excellent performance in enhancing the photostability of poly(p-phenylene sulfide), *RSC Adv.*, 2017, **7**, 21758–21767.

67 B. Biswas, N. R. Bandyopadhyay and A. Sinha, Mechanical and dynamic mechanical properties of unsaturated polyester resin-based composites, in *Unsaturated Polyest. Resins*, Elsevier, 2019, pp. 407–434, DOI: **10.1016/B978-0-12-816129-6.00016-8**.

68 K. P. Menard and N. R. Menard, Dynamic mechanical analysis in the analysis of polymers and rubbers, in *Encycl.*

*Polym. Sci. Technol.*, Wiley, 2015, pp. 1–33, DOI: **10.1002/0471440264.pst102.pub2**.

69 A. Badawi, Characterization of the optical and mechanical properties of CdSe QDs/PMMA nanocomposite films, *J. Mater. Sci. Mater. Electron.*, 2015, **26**, 3450–3457, DOI: **10.1007/s10854-015-2854-1**.

70 A. Ahmed, B. Adak, T. Bansala and S. Mukhopadhyay, Green solvent processed cellulose/graphene oxide nanocomposite films with superior mechanical, thermal, and ultraviolet shielding properties, *ACS Appl. Mater. Interfaces*, 2020, **12**, 1687–1697, DOI: **10.1021/acsami.9b19686**.

71 H. Liu, N. Li, M. Feng, G. Li, W. Zhang and T. An, Near-infrared light induced adsorption–desorption cycle for VOC recovery by integration of metal–organic frameworks with graphene oxide nanosheets, *Environ. Sci. Nano*, 2022, **9**, 1858–1868, DOI: **10.1039/D2EN00103A**.

72 R. Miraftab, B. Ramezanzadeh, G. Bahlakeh and M. Mahdavian, An advanced approach for fabricating a reduced graphene oxide-AZO dye/polyurethane composite with enhanced ultraviolet (UV) shielding properties: experimental and first-principles QM modeling, *Chem. Eng. J.*, 2017, **321**, 159–174, DOI: **10.1016/j.cej.2017.03.124**.